

# The lensing and temperature imprints of voids on the Cosmic Microwave Background

Yan-Chuan Cai<sup>1\*</sup>, Mark Neyrinck<sup>2,3,4,5</sup>, Qingqing Mao<sup>6</sup>, John A. Peacock<sup>1</sup>, Istvan Szapudi<sup>7</sup>, Andreas A. Berlind<sup>6</sup>

<sup>1</sup> *Institute for Astronomy, University of Edinburgh, Royal Observatory, Blackford Hill, Edinburgh, EH9 3HJ, UK*

<sup>2</sup> *Institute for Computational Cosmology, Department of Physics, Durham University, South Road, Durham DH1 3LE, UK*

<sup>3</sup> *Institut d'Astrophysique de Paris, 98 bis bd Arago, 75014, Paris, France*

<sup>4</sup> *Sorbonne Universites, UPMC Univ Paris 6 et CNRS, UMR 7095, Paris, France*

<sup>5</sup> *Department of Physics and Astronomy, The Johns Hopkins University, Baltimore, MD 21218, USA*

<sup>6</sup> *Department of Physics and Astronomy, Vanderbilt University, Nashville, TN 37235, USA*

<sup>7</sup> *Institute for Astronomy, University of Hawaii, 2680 Woodlawn Drive, Honolulu, HI, 96822*

19 December 2016

## ABSTRACT

We have searched for the signature of cosmic voids in the CMB, in both the Planck temperature and lensing-convergence maps; voids should give decrements in both. We use ZOBOV voids from the DR12 SDSS CMASS galaxy sample. We base our analysis on  $N$ -body simulations, to avoid a *posteriori* bias. For the first time, we detect the signature of voids in CMB lensing: the significance is  $3.2\sigma$ , close to  $\Lambda$ CDM in both amplitude and projected density-profile shape. A temperature dip is also seen, at modest significance ( $2.3\sigma$ ), with amplitude about 6 times the prediction. This temperature signal is induced mostly by voids with radius between 100 and 150  $h^{-1}$ Mpc, while the lensing signal is mostly contributed by smaller voids – as expected; lensing relates directly to density, while ISW depends on gravitational potential. The void abundance in observations and simulations agree, as well. We also repeated the analysis excluding lower-significance voids: no lensing signal is detected, with an upper limit of about twice the  $\Lambda$ CDM prediction. But the mean temperature decrement now becomes non-zero at the  $3.7\sigma$  level (similar to that found by Granett et al.), with amplitude about 20 times the prediction. However, the observed dependence of temperature on void size is in poor agreement with simulations, whereas the lensing results are consistent with  $\Lambda$ CDM theory. Thus, the overall tension between theory and observations does not favour non-standard theories of gravity, despite the hints of an enhanced amplitude for the ISW effect from voids.

**Key words:** large-scale structure of Universe – gravitational lensing: weak – methods: observational – cosmic background radiation

## 1 INTRODUCTION

In a  $\Lambda$ CDM universe, dark energy stretches cosmic voids, causing their gravitational potential to decay. Photons from the Cosmic Microwave background (CMB) then lose energy when traversing a void, so that the CMB temperature is expected to be colder when a void sits along the line of sight. This is the Integrated Sachs-Wolfe effect (ISW: Sachs & Wolfe 1967), and its detection would give direct evidence of dark energy, at least for large voids that evolve quasi-linearly. But this imprint has not been detected with unquestionable significance, owing to the large effective noise term from the superimposed primordial CMB temperature fluctuations. This noise can be reduced by stacking CMB imprints from many voids,

and several papers have followed such a strategy (Granett et al. 2008; Ilić et al. 2013; Cai et al. 2014; Planck Collaboration et al. 2014, 2015c; Hotchkiss et al. 2015).

The highest S/N measurement of this kind was reported in Granett et al. (2008; G08). They stacked the WMAP7 temperature maps for 50 voids from the SDSS DR6 galaxy sample, yielding a temperature decrement of approximately  $-10\mu K$  at the  $3.7\sigma$  level. This signal is rather high compared to expectations from  $\Lambda$ CDM, but the result was reproduced with the same G08 catalogue using Planck CMB temperature maps (Planck Collaboration et al. 2014, 2015c). A limitation of G08 is that their voids were found in a photometric redshift catalogue, with large redshift uncertainties compared to spectroscopic redshift samples. But the photometric-redshift smearing may even help to detect very elongated structures along the line of sight, which may have the highest ISW sig-

\* E-mail: y.c.cai@durham.ac.uk

nals (Granett et al. 2015). Our goal in the present study is therefore to conduct a similar analysis using the larger SDSS-DR12 CMASS spectroscopic redshift sample, which covers the same redshift range ( $0.4 < z < 0.7$ ) and the same volume as that of the DR6 photometric redshift sample in the NGC region. We also include the SGC region from the CMASS sample in this study.

A number of ISW searches using voids from the SDSS DR7 spectroscopic redshift samples at low  $z$  found less significant results, i.e. at around the  $2\sigma$  level (Ilić et al. 2013; Cai et al. 2014; Planck Collaboration et al. 2014), or a null detection (Hotchkiss et al. 2015). All of these studies used the ZOBOV algorithm (Neyrinck et al. 2005; Neyrinck 2008) to find voids. The variety of results reported by different groups is largely due to the differences in the way void catalogues are pruned. This suggests that the details of void selection are important for studies of this kind.

A number of factors may affect the stacked ISW signal. First, voids found in the galaxy field may not necessarily correspond to sites of maximal coldness in the ISW signal (potential maxima, in linear theory). There may be spurious voids due to the discreteness of the galaxy sample. Second, the edges of voids in over-dense environments (the so-called voids-in-clouds: Sheth & van de Weygaert 2004) may be contracting. Their underlying potentials are negative rather than positive at the scale of the void, which reverses the sign of the ISW signal (Cai et al. 2014). Finally, it is important to note that the selection of voids has to be conducted on physical grounds *prior* to the measurement of the signal. Failure to do so can introduce *a posteriori* bias and over-estimation of the statistical significance of the measurement. The above issues can either introduce noise or cause biases for the ISW signal. They can be reduced to some extent by calibrating the void catalogues using simulations, as demonstrated in Cai et al. (2014).

In this paper we analyse voids found in the SDSS-DR12 CMASS sample, following a procedure similar to that of Cai et al. (2014). Furthermore, we also carry out a stacking analysis using the Planck lensing convergence map. Even though CMB lensing is dominated by structures at  $z \simeq 2$ , low- $z$  structures also contribute. Voids should be associated with density minima in order to cause an ISW temperature decrement, and this underdensity should be detectable via CMB lensing. Weak gravitational lensing by voids has been predicted in the literature (Amendola et al. 1999; Krause et al. 2013; Higuchi et al. 2013) and it has been measured using weak galaxy shear (Melchior et al. 2014; Clampitt & Jain 2015; Gruen et al. 2016; Sánchez et al. 2016). But for the more distant galaxies, the use of CMB lensing should be a better probe.

Evidence for the co-existence of the ISW and CMB lensing signals would help to confirm the reality of each effect. This dual probe is valuable from the point of view of modified gravity, since the two effects are closely related: lensing depends on the sum of metric potentials  $\Phi + \Psi$ , whereas ISW depends on the time derivative of this same combination. Hints of the general coexistence of both the ISW and CMB lensing signatures have been found by Planck Collaboration et al. (2015c). This paper also showed some evidence for a mean lensing signal from the G08 supervoids (but not from the G08 superclusters). This is the issue that we intend to explore in more detail, with a larger void sample.

This paper is organised as follows: In Section 2, we define our void catalogues and describe our simulations for the ISW and lensing signal associated with voids. Section 3 presents the main results of stacking voids with the CMB temperature map and the lensing convergence map, focusing on the estimation of signal-to-noise. We conclude and discuss our results in Section 4.

## 2 VOID DEFINITION FROM DR12 AND SIMULATIONS

### 2.1 The CMASS void sample

We use a void catalogue produced from the Baryon Oscillation Spectroscopic Survey (BOSS: Dawson et al. 2013), Data Release 12 (DR12), the final data release. It is part of the third generation of the Sloan Digital Sky Survey (SDSS-III: Eisenstein et al. 2011). We here briefly describe the void catalogue, based on the watershed and point-sample-based void finder ZOBOV (Neyrinck 2008). Greater detail can be found in Mao et al. (2015).

We use voids from BOSS DR12 large-scale structure (LSS) galaxy catalogues. BOSS galaxies were uniformly targeted in two samples:  $z < 0.45$  (LOWZ) and one at  $0.4 < z < 0.7$  that was designed to be approximately volume-limited in stellar mass (CMASS). Redshift cuts  $0.2 < z < 0.43$  on the LOWZ sample and  $0.43 < z < 0.7$  on the CMASS sample were applied to ensure clear geometric boundaries and no overlap between samples. Both the North and South regions of the sample were included, and we focus on using the CMASS sample in this work. A study in the LOWZ volume with spectroscopic redshifts was conducted by Ilić et al. (2013); Cai et al. (2014); Planck Collaboration et al. (2014) using the SDSS DR7 galaxy sample. There was no attempt to mimic a volume-limited sample; instead, following Granett et al. (2008), local densities were compared to an observed radial density distribution  $n(z)$ , dividing out the radial selection function.

The ZOBOV void finder locates density depressions using a Voronoi tessellation to measure each galaxy’s density and that of its neighbours. Neighbouring Voronoi cells are grouped into ‘zones’ (local density depressions) with a watershed algorithm. Another watershed step is necessary to join some of the zones together, to find the largest-scale voids. Mao et al. (2015) used ZOBOV in its ‘fully parameter-free’ mode, the results consisting of a hierarchical set of voids and subvoids, not necessarily disjoint. From this hierarchy, they discarded the top few voids, which had volume of order the volume of the survey. The largest remaining voids still have quite large volumes and irregular shapes, consisting of many smaller density depressions. As we describe below, we found that these irregular shapes caused their volume centroids to poorly estimate the peaks of their ISW signals, giving the counterintuitive result that the apparently largest, deepest voids have unreliable ISW signals, both in mock catalogues and in observations. Including fewer subvoids at the edges of the largest voids would be more likely to give a reliable detection. The effective radius of a void is defined as  $r_v \equiv (3V/4\pi)^{1/3}$ , where  $V$  is the sum of Voronoi volumes of all galaxies in the void.

ZOBOV returns a statistical significance for each void, based on the ratio of the lowest density on the void edge  $\rho_{\text{ridge}}$  to the density minimum at the void centre  $\rho_{\text{min}}$ . This ratio is compared to its distribution in a Poisson set of particles. In our analysis, we will use all voids regardless of their significance. We also test the highest-contrast voids, with significance estimated to be  $> 3\sigma$  compared to a Poisson sample, as in G08. But note that the Poisson noise criterion is probably more meaningful in the photometric than spectroscopic case, since the approximation of a Poisson-sampled smooth field is more relevant in the photometric case. The spectroscopic sample is sparser, but each galaxy has a well-defined position.

Voids with relatively high significance also tend to have deeper central underdensities. We find that all voids passing the  $3\sigma$  selection criterion have density minima more negative than  $-0.45$ . We weight Voronoi cells belonging to each void by their volumes in order to define the void centre – although possibly a void’s centre might correspond best to the peak ISW signal if

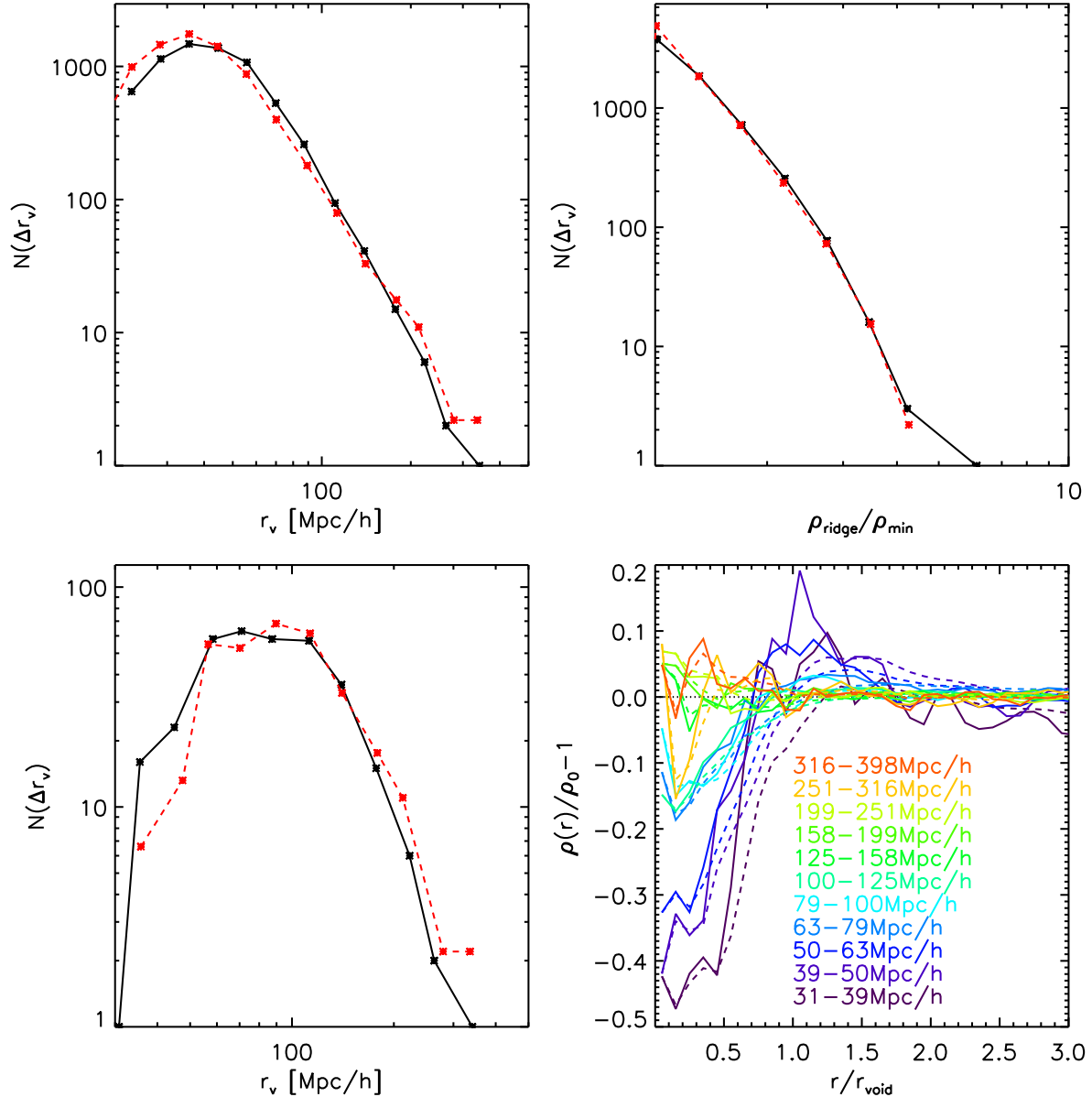


**Figure 1.** Left: the number of voids in logarithmic bins of void radius. Black solid and red dashed lines represents results from the CMASS sample and from our HOD mocks (after rescaling by the effective volume of the CMASS sample at the BAO scale; see the text for more details) respectively. The bottom-left panel shows voids passing the  $3\sigma$  significance criterion, defined as  $\rho_{\text{ridge}}/\rho_{\text{min}} > 2$ . Top-right: similar to the left but showing number of voids versus  $\rho_{\text{ridge}}/\rho_{\text{min}}$  (see the text for more details). The bottom-right panel shows the dark matter density profiles for the simulated voids from the bottom-left. Dashed curves represent cumulative profiles. Different colours indicate different ranges of radius.

we used its ‘circumcentre,’ the centre of the lowest-density Delaunay cell around the void’s minimum-Voronoi-density galaxy (Nadathur & Hotchkiss 2015).

## 2.2 The mock void catalogue

To calibrate our void catalogue for the ISW detection, we generate mock catalogues using haloes from an  $N$ -body simulation. The simulation was run in the concordance cosmology ( $\Omega_m = 0.24$ ,  $\Omega_\Lambda = 0.76$ ,  $n_s = 0.958$ ,  $\sigma_8 = 0.77$ ,  $h = 0.73$ ; Li et al. 2013). The box size of the simulation is  $L = 1000 h^{-1} \text{Mpc}$ , with  $N_p = 1024^3$  particles. The volume of the simulation is approxi-

mately a factor of 2.2 smaller than that of the CMASS sample, but as we show in Fig. 1, the abundance of simulated voids agrees very well with observations, suggesting that this simulation is reasonably representative of the CMASS sample.

We use a 5-parameter halo occupation distribution (HOD) (Seljak 2000; Peacock & Smith 2000; Scoccimarro et al. 2001; Berlind & Weinberg 2002; Zheng et al. 2005) with best-fitting parameters for the CMASS sample from White et al. (2011) [see also Manera et al. 2013] to populate the haloes that consist of more than 20 particles. The number density of HOD galaxies is  $0.0004(h^{-1} \text{Mpc})^{-3}$ , which is a good match to the peak number density of the CMASS sample. Note that the CMASS sample is

not a volume-limited sample: its number density varies with redshift. When we plot the abundance against the significance of voids, defined by the ratio of the lowest density on the ridge  $\rho_{\text{ridge}}$  versus the minimal density of the void  $\rho_{\text{min}}$ , the agreement is also very good between the simulation and observation (top-right of Fig. 1). It is even more striking to find that the agreement persists for the very small subset of voids shown by the bottom-left panel of Fig. 1, where we select only voids that are  $3\sigma$  above the Poisson fluctuations.

Note that we have adopted the effective volume of the CMASS sample at the BAO scale with  $P_0 = 2 \times 10^4 (h^{-1}\text{Mpc})^3$  specified in Cuesta et al. (2016), which is approximately  $2.2(h^{-1}\text{Gpc})^3$  for the comparison with simulations. If we used the total volume of CMASS,  $10.8 \text{ Gpc}^3$  (Cuesta et al. 2016), assuming  $h = 0.7$ , the red dashed curves in Fig. 1 would need to be boosted by a factor 1.6. We attribute this factor to the sparseness of the sample in the near and far parts of the survey, unlike in our uniform-selection-function mock.

To get some idea of how a non-uniform selection function affects our measurement, we have also subsampled our HOD galaxies to qualitatively mimic the CMASS line-of-sight selection function. We do this by applying a 1D sinusoidal sampling fluctuation to the box: the sampling peaks in the centre, and falls to 1/4 of the peak at the ‘line-of-sight’ edges. Putting the sinusoidal fluctuation along the three axes, and shifting it by half a wavelength, gives us six (not independent) mocks from the simulation. We also add redshift-space distortions for the HOD galaxies at the level of centre-of-mass velocities for haloes. The resulting void sample has a similar void abundance function to the one from the volume-limited sample, but its overall amplitude is slightly reduced, again supporting the idea that this sampling difference is behind the factor of 1.6 in the void volume functions. The agreement with the CMASS sample is still reasonable when the  $10.8 \text{ Gpc}^3$  volume of CMASS is accounted for. We have also checked that the simulated ISW and lensing  $\kappa$  signals from this mock sample remains similar to those derived from the volume-limited sample. We therefore use the mock void catalogue from the volume limited sample, since it has slightly better statistics. The good match between the simulated and observed void populations gives us confidence in our modelled ISW and lensing signals.

The bottom-right panel of Fig. 1 shows examples of the void density profiles from simulations, with the dashed curves showing the cumulative profiles. There is a trend that void centres become shallower with increasing void radius, while small voids are more compensated by over-dense ridges. It is striking that the largest voids ( $r_v > 150 h^{-1}\text{Mpc}$ ) are not in fact strongly underdense. This behaviour probably arises because the largest voids arise via the merging of many neighbouring voids, the collection having a possibly quite irregular shape. The volume-weighted centre becomes ill-defined, and less appropriate for estimating peaks in the ISW and lensing signal. Based on this, we exclude voids with  $r_v > 150 h^{-1}\text{Mpc}$  in both simulation and observations. We also exclude voids with  $r_v < 20 h^{-1}\text{Mpc}$  from our analysis, which corresponds to an angular radius of about one degree. Voids smaller than this are relatively few and do not have any noticeable effect on our results. With these selections, we have 6723 voids out of the 7401 in total. Applying the  $3\sigma$  cut based on the significance of voids leaves us with 307 voids.

### 2.3 Simulating the ISW and lensing $\kappa$ signal

To simulate the ISW signal, we compute the time derivative of the potential  $\dot{\Phi}$  using the particle positions and velocities in Fourier space (Seljak 1996; Cai et al. 2009; Smith et al. 2009; Cai et al. 2010):

$$\dot{\Phi}(\vec{k}, t) = \frac{3}{2} \left( \frac{H_0}{k} \right)^2 \Omega_m \left[ \frac{\dot{a}}{a^2} \delta(\vec{k}, t) + \frac{i\vec{k} \cdot \vec{p}(\vec{k}, t)}{a} \right], \quad (1)$$

where  $\vec{p}(\vec{k}, t)$  is the Fourier transform of the momentum density divided by the mean mass density,  $\vec{p}(\vec{x}, t) = [1 + \delta(\vec{x}, t)]\vec{v}(\vec{x}, t)$ , and  $\delta(\vec{k}, t)$  is the Fourier transform of the density contrast.  $H_0$  and  $\Omega_m$  are the present values of the Hubble and matter density parameters. The inverse Fourier transform of the above yields  $\dot{\Phi}$  in real space on 3D grids. The integration of  $\dot{\Phi}$  along the line of sight yields the ISW and Rees-Sciama (Rees & Sciama 1968) temperature fluctuations:

$$\Delta T(\hat{n}) = \frac{2}{c^2} \int \dot{\Phi}(\hat{n}, t) dt, \quad (2)$$

where  $c$  is the speed of light. We use the simulation output at  $z = 0.43$  and integrate through the entire simulation box for each void to obtain  $\Delta T(\hat{n})$ . Note that voids can influence the potential even when outside the survey. For the highest potential hills in linear theory, Granett et al. (2009) found that neglecting the ISW contribution from areas outside the DR7 survey used in G08 can underestimate extrema in the ISW signal by a factor of up to  $\sim 2$ . This is why detailed simulations are essential in order to predict the expected signal.

To simulate the CMB lensing convergence signal  $\kappa$ , we use the same simulation output and project all the mass in each simulation box to obtain the 2D convergence map using

$$\kappa(x, y) = \frac{3H_0^2\Omega_m}{2c^2} \int_{D_{L1}}^{D_{L2}} \frac{(D_S - D_L)D_L}{D_S} \frac{\delta(x, y, D_L)}{a} dD_L, \quad (3)$$

where  $D_L$  and  $D_S$  are the comoving distances of the lens and the source, which is the distance to the last scattering surface for the case of CMB lensing.  $\delta$  is the 3D density contrast from our simulations. We approximate the redshift of the lens by the median redshift  $z \sim 0.55$  of the CMASS sample. We also tried drawing redshifts for each simulated void from the observed redshift distribution of the CMASS void sample and repeating the above calculation. This made a negligible difference to the predicted signal.

The simulations that we use do not provide an output exactly at our desired average redshift of 0.55:  $z = 0.43$  is the closest. They also have a slightly smaller value of  $\Omega_m$  than the Planck best-fit value. Structure grows from  $z = 0.55$  to  $z = 0.43$  by  $\sim 6\%$  according to linear theory, and the linear growth factor of the ISW also changes by a similar amount. So the effect of the slight offset in redshift should be negligible. We have calculated distances assuming the Planck cosmology. The predicted amplitude of the lensing signal is again insignificantly higher when using the Planck cosmology as compared with the parameters of the original simulation.

To reduce the sample variance, we project the data cubes of  $\dot{\Phi}$  and  $\delta$  along all the three Cartesian axes of the simulation box for each void. 2D compensated top-hat filters are applied to the 2D ISW and  $\kappa$  maps respectively at the location of each void. The expected ISW and lensing  $\kappa$  signals from our simulations are plotted in dashed curves in the top panels of Figs 2-5.

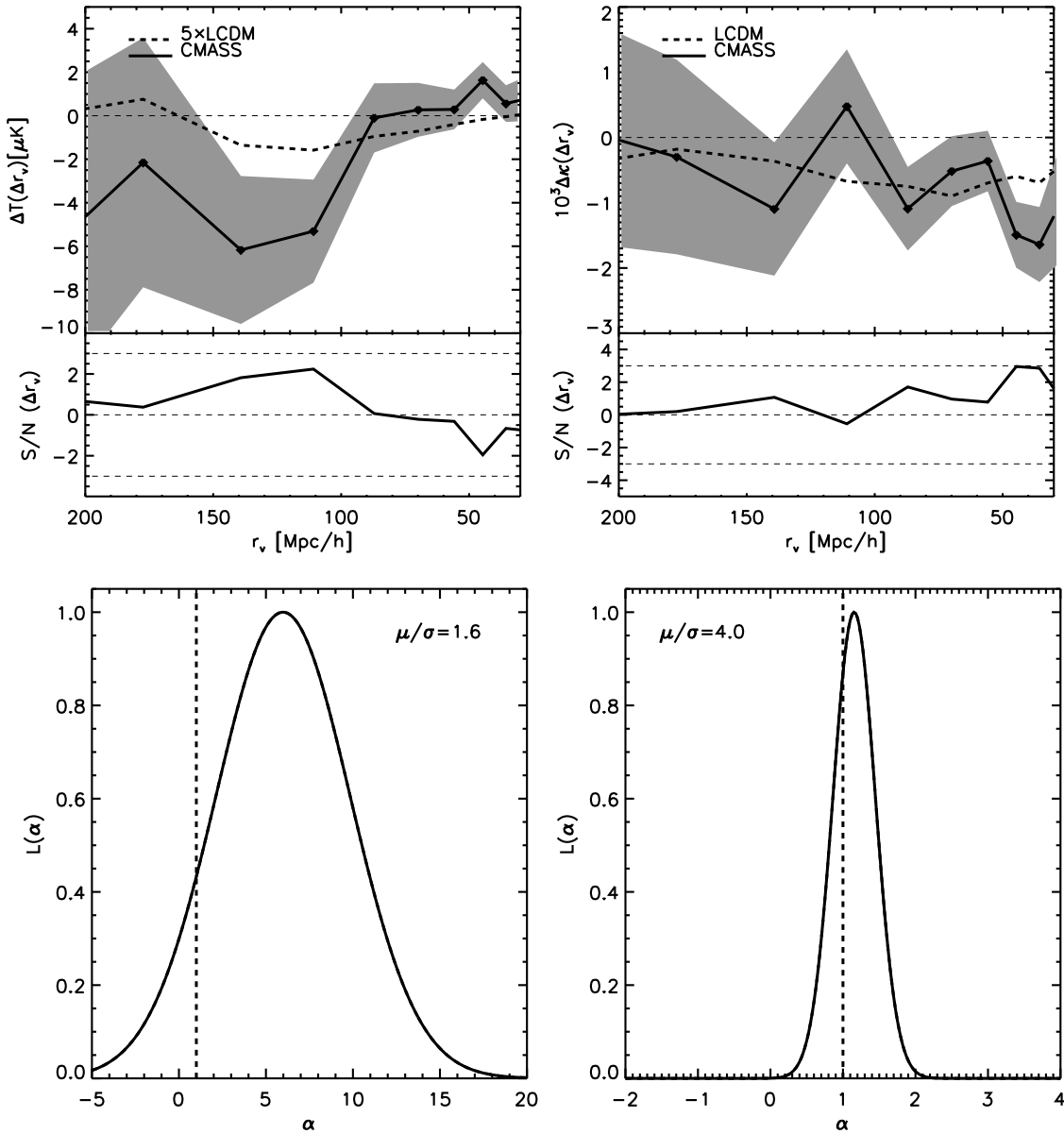


**Figure 2.** Differential (top-left) stacked-filtered CMB temperatures associated with voids. Voids are sorted in descending order of radii. The grey regions are the  $1\sigma$  error estimated from 1000 simulated CMB maps. The simulation curve (black dashed) on the top-left has now been multiplied by a factor of 5 for better illustration. Their bottom panels shows the corresponding signal-to-noise. The thick-dash curve is the theoretical prediction from the  $\Lambda$ CDM universe using  $N$ -body simulations. The top-right figure is similar to the left but showing results from stacking the CMB lensing  $\kappa$  map from Planck. Both the CMB temperature maps and the lensing  $\kappa$  map have their power at  $\ell < 10$  set to be zero to help reduce cosmic variance. Bottom figures: the likelihood functions  $\mathcal{L}(\alpha)$  for the CMB temperature and lensing  $\kappa$  results. The  $\mu$  and  $\sigma$  values are the best-fit values of the mean and variance with a Gaussian function for the likelihoods. The default choice with all voids included has  $1.6\sigma$  deviation from zero temperature and  $4.0\sigma$  for  $\Delta\kappa$ . This high-significance lensing signal is dominated by voids smaller than  $50 h^{-1}\text{Mpc}$ , whereas the hint of a temperature signal comes only from larger voids, in the range  $100\text{--}150 h^{-1}\text{Mpc}$ . The dashed vertical lines in the lower panels show the predicted signal:  $\alpha = 1$ , where  $\alpha$  is a free scaling parameter applied to the  $\Lambda$ CDM prediction.

### 3 STACKING VOIDS FOR THE CMB TEMPERATURE AND LENSING MAPS

Given the void catalogues defined in the previous section, we now stack the CMB temperature and lensing  $\kappa$  maps around the void centres. We use Planck foreground-cleaned CMB temperature maps generated from different component separation methods: SMICA, COMMANDER, SEVEM and NILC (Planck Collaboration et al. 2015e). No difference in the results from different temperature maps are found; We have also re-

peated our analyses with the thermal SZ  $y$ -map from Planck (Planck Collaboration et al. 2015d), finding that the residual SZ signal at the sky positions of voids, if any, is at the sub- $\mu K$  level, which is negligible. We present results using the SEVEM map in practice. A common mask UT78 is applied to both the temperature and lensing maps (Planck Collaboration et al. 2015a). The lensing situation offers less choice, as only a single convergence map is available: the 2015 lensing data are released directly in the form of the spherical harmonic transform of the (masked)  $\kappa$  field (Planck Collaboration et al. 2015b).

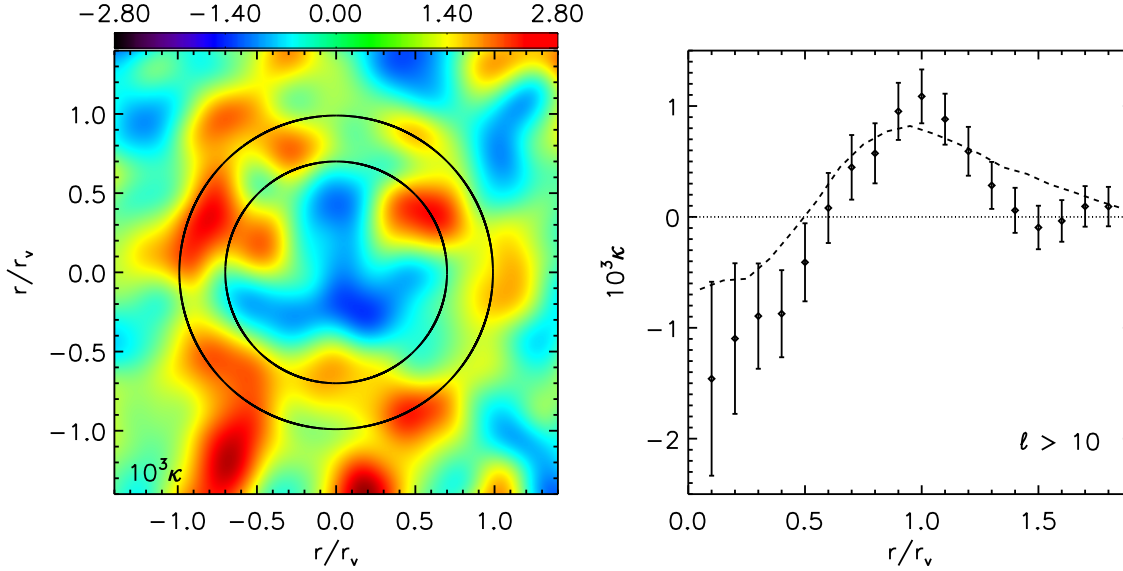


**Figure 3.** Left: Stacked Planck lensing  $\kappa$  maps using all voids with  $r_v > 20 h^{-1}\text{Mpc}$ : ‘up’ is the direction of Galactic north. Right: 1D  $\kappa$  profile for the left panel. Errors about the mean are plotted on the right panel, and the dashed line shows the predictions of our mocks. The CMB  $\kappa$  maps are rescaled by the void radius  $r_v$  before stacking. The inner and outer circles have the radii of  $r_v/\sqrt{2}$  and  $r_v$  respectively. They represent the optimal filter radius we found from the HOD mock.

### 3.1 The optimal radius of the filter

Corresponding to each void centre, the CMB signal is taken to be the averaged temperature  $T$  (or  $\kappa$ ) within a circular aperture  $r < R_{\text{filter}}$  minus the same quantities averaged over an annular aperture  $R_{\text{filter}} < r < \sqrt{2}R_{\text{filter}}$ , where  $R_{\text{filter}}$  is the size of the compensated top-hat filter. We will call the filtered temperature and lensing convergence  $\Delta T$  and  $\Delta\kappa$ , i.e.

$$\begin{aligned} \Delta T &= \frac{\int_0^{R_{\text{filter}}} T(\mathbf{r}) d\mathbf{r}}{\int_0^{R_{\text{filter}}} d\mathbf{r}} - \frac{\int_{R_{\text{filter}}}^{\sqrt{2}R_{\text{filter}}} T(\mathbf{r}) d\mathbf{r}}{\int_{R_{\text{filter}}}^{\sqrt{2}R_{\text{filter}}} d\mathbf{r}} \\ \Delta\kappa &= \frac{\int_0^{R_{\text{filter}}} \kappa(\mathbf{r}) d\mathbf{r}}{\int_0^{R_{\text{filter}}} d\mathbf{r}} - \frac{\int_{R_{\text{filter}}}^{\sqrt{2}R_{\text{filter}}} \kappa(\mathbf{r}) d\mathbf{r}}{\int_{R_{\text{filter}}}^{\sqrt{2}R_{\text{filter}}} d\mathbf{r}} \end{aligned} \quad (4)$$

To maximise the ISW signal, Cai et al. (2014) showed that the optimal choice was  $R_{\text{filter}} = 0.6r_v$ , using mock void catalogues defined via haloes from  $N$ -body simulations. Using our HOD mocks, we re-investigate this scale factor for a possible dependence on void radius. We find that  $R_{\text{filter}} = 0.7r_v$  gives slightly higher amplitudes for the stacked filtered  $T$  signal as well as for the lensing  $\kappa$  signal for voids with  $100 < r_v < 150 h^{-1}\text{Mpc}$ . The corresponding outer radius of the filter is  $r_v$ . For simplicity, we will use this size of the filter throughout our analysis, even though it may not be the optimal choice for all ranges of voids.

### 3.2 Stacking with all voids

We now look at the results of stacking the CMB sky at the DR12 void locations. Because the predicted signal varies with void radius, as does the fidelity of the void catalogue, we divided the results into different bins of void radius. We sorted the voids in decreasing order of radius, and measured the average filtered  $\Delta T$  and  $\Delta\kappa$  imprints for several logarithmically-spaced bins of  $r_v$ .

The results are shown in the top row of Fig. 2. The filtered temperature  $\Delta T$  is negative at large void radii. The deepest temperature dip is approximately  $-6\mu\text{K}$  between  $r_v \simeq 100$  to  $150 h^{-1}\text{Mpc}$ ,

with a significance of  $2.4\sigma$ .  $\Delta T$  crosses zero at  $r_v \simeq 90 h^{-1}\text{Mpc}$  and remains slightly positive at smaller void radii. We can understand the presence of positive filtered temperature as an indication of voids-in-clouds, i.e. voids living in over-dense environments. The gravitational potential at the scale of the void for a void-in-cloud is negative; i.e., it is a potential well rather than a potential hill as intuitively expected for a void. The dominant linear ISW effect thus yields a positive temperature perturbation (Cai et al. 2014). We also find that the simulated ISW signal crosses zero, though at a similar void radius of  $\approx 30 h^{-1}\text{Mpc}$ . This indicates that the stacked signal for the CMB temperature qualitatively resembles an ISW signal in a  $\Lambda\text{CDM}$  universe.

For the largest voids, the observed  $\Delta T$  shows consistency with zero at  $r_v \gtrsim 150 h^{-1}\text{Mpc}$ , which confirms our speculation from simulations that these objects may not be truly underdense at their volume centroids. This could happen because the few largest voids can be highly irregular in shape, composed of a few density depressions linked together. Interestingly, the shape of the observed  $\Delta T$  appears similar in shape to the simulation results, although the simulated  $\Delta T$  needs to be scaled up in order to match the data shown in Fig. 2 (We discuss this point below).

When we look at the same results with the CMB lensing  $\kappa$  map, as shown in the top-right panel of Fig. 2, the  $\Delta\kappa$  signal has a different character from that of  $\Delta T$ . The  $\kappa$  measurements are noisy at the radii where  $\Delta T$  peaks; but within the errors they follow closely the curve from our simulations, and the amplitude of the signal increases with decreasing void radius. The minimum of  $\Delta\kappa$  has a significance of  $\approx 3\sigma$  at  $r_v \approx 30 h^{-1}\text{Mpc}$ .

Fig. 3 shows the stacked  $\kappa$  map (left) and its profile (right) from the entire void sample. An underdensity of  $\kappa$  surrounded by a ring of over-density is clearly seen. The mean value of  $\kappa$  is of order  $-10^{-3}$  near the centre, and crosses zero at  $\approx 0.6r_v$ , which is very close to the optimal filter radius found from our simulation for the ISW signal. At even larger radii, the over-dense ridge is centred very closely at  $r_v$  and then it drops to the background at  $\approx 1.4r_v$ . Overall, the profile resembles that of a void-in-cloud. This is ex-

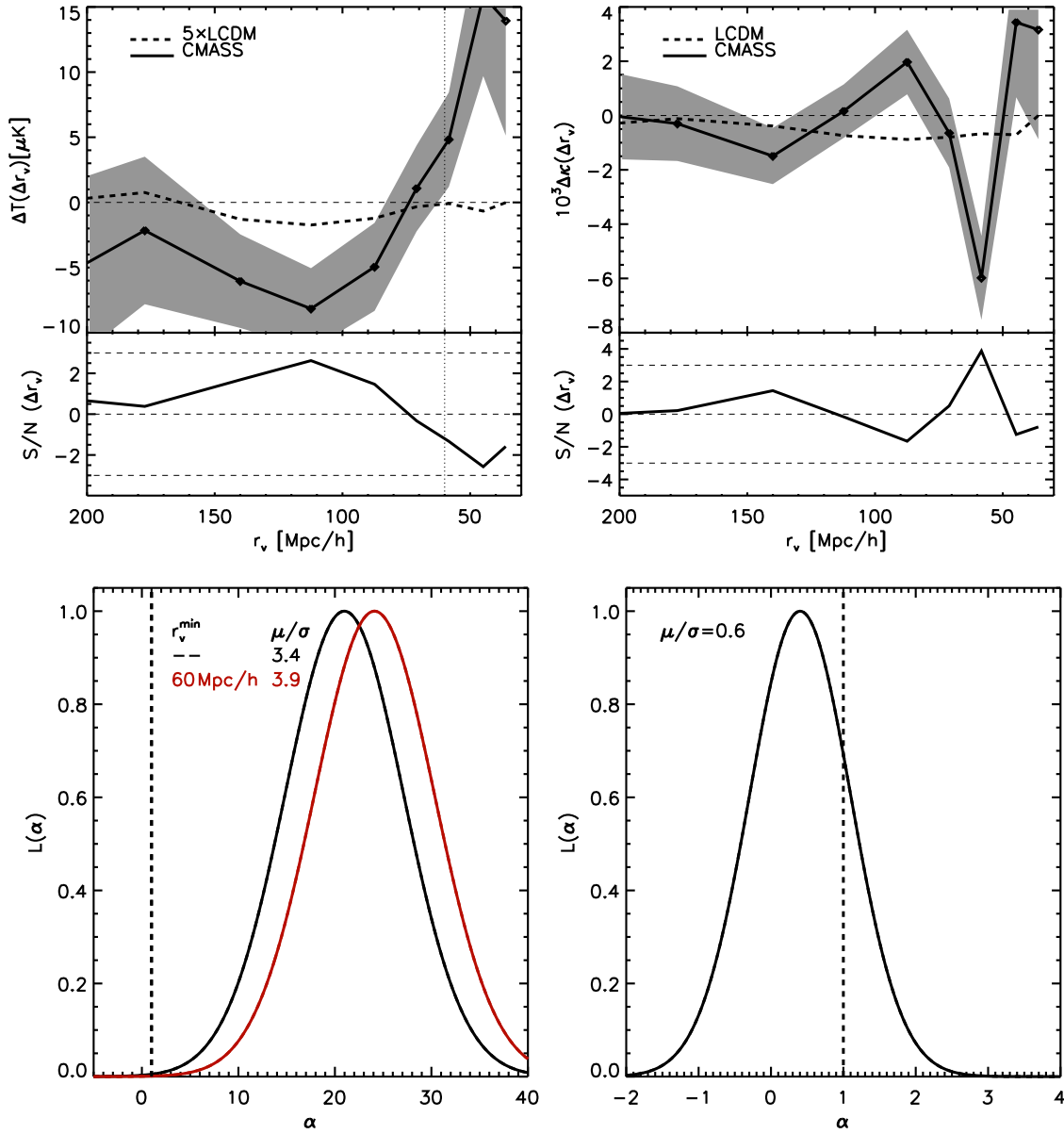


**Figure 4.** Similar to Fig. 2 but showing results with voids that are  $3\sigma$  above Poisson fluctuations, the same selection as in Granett et al. (2008). The vertical thin-dash curve indicate the zero point for the simulated ISW signal. The default choice with all voids with  $r_v < 150 h^{-1}\text{Mpc}$  included has  $3.4\sigma$  deviation from zero temperature and the  $\Delta\kappa$  result is consistent with zero. When using the zero-crossing from simulations as the lower limit, the significance for  $\Delta T$  increases to  $3.9\sigma$ .

pected as the population is dominated by small voids, which are more likely to live in over-dense environments. The dashed curve in the right-hand panel shows the prediction for the lensing convergence profile from our simulated voids. It agrees well with the observations within the errors.

To quantify the significance of the stacked signal, we utilise the model predictions given by our simulations of a  $\Lambda\text{CDM}$  universe for both the ISW  $\Delta T$  and lensing  $\Delta\kappa$ . We assume that the probability of having the observed  $\Delta T$  and  $\Delta\kappa$  given the model from simulations with a range of values for the amplitude parameter  $\alpha$  is  $\mathcal{L}(\alpha)$ , where

$$\ln[\mathcal{L}(\alpha)] = - \sum_{i=1}^N \left[ (D_i^{\text{obs}} - \alpha M_i^{\text{sim}})^2 / (2\sigma_i^2) \right]. \quad (5)$$

$D_i^{\text{obs}}$  and  $M_i^{\text{sim}}$  are the observed and simulated quantities of either  $\Delta T$  or  $\Delta\kappa$  for each void. The subscript  $i$  indicates a given void and  $N$  is the total number of voids.  $\sigma_i$  is the  $1\sigma$  error for each void estimated from 1000 simulated CMB maps of  $T$  and  $\kappa$ . These errors include all sources of cosmic variance, since the mock datasets discussed in Section 2.2 automatically include void-to-void variations and line-of-sight projections of large-scale structure. But our simulated foreground maps are overlaid with a simulation of the general level of fluctuations seen in the CMB temperature and lensing maps, and these latter effects dominate the noise in practice. The normalized probabilities for  $\alpha$  are given at the bottom of Fig. 2. We do not use voids with  $r_v > 150 h^{-1}\text{Mpc}$  for reasons explained in the previous section. With this choice, we find  $1.6\sigma$  and  $4\sigma$  deviations from null for the temperature and lensing stacked results

respectively from the data. We have also tried allowing voids as large as  $r_v = 250 h^{-1}\text{Mpc}$  to be included, finding that the significance of the filtered temperature and lensing signal remains about the same. Note that the signal of each void is effectively weighted by the square of its signal-to-noise. The expected signal-to-noise is greater for large voids, so voids with larger radii contribute more per void to the likelihood.

The signal-to-noise estimation using equation (5) ignores any covariance between voids in different size bins. We think this should be a good approximation: the empirical noise in the CMB maps is on 1-degree scales for temperature and smaller scales for lensing, whereas the typical separation of voids is larger than this. Also, note that the covariance in the compensated-filtered temperature measured from random simulations from void to void can be positive or negative, depending in a possibly complicated way on the sizes of the voids and their separation. Nevertheless, we have double-checked the signal-to-noise using a second method where all voids are rescaled and stacked together to yield a single average  $T$  or  $\kappa$  value. In this case, any covariance effects would automatically be included in the error bar estimated via our simulations. Moreover, this method requires no theoretical prior. We find that the  $S/N$  values estimated in this way are 2.3 and 3.2 for the temperature and  $\kappa$  results respectively. These are slightly different to the figures estimated using equation (5), but the qualitative conclusion is the same: strong evidence for a lensing signal, but only a marginal indication of a temperature signal.

In summary, without any trimming of the void catalogue, there is only a  $2.3\sigma$  ( $1.6\sigma$  when neglecting void-to-void covariance) hint of cold ISW imprints of voids on the CMB. Any signal is contributed mostly by large voids with  $r_v > 100 h^{-1}\text{Mpc}$  – and the amplitude in this regime is more than 10 times larger than the  $\Lambda\text{CDM}$  prediction. But very little signal is seen from smaller voids, so that the overall best-fitting amplitude is about 6 times the prediction (although the likelihood ratio between this signal level and the unscaled prediction is only 2.5). There is a much stronger ( $3.2\sigma$ ) ( $4.0\sigma$  when neglecting void-to-void covariance) significance for the measurement of the CMB lensing signal, which is contributed by smaller voids, and there is close agreement in shape and amplitude between data and simulation. Thus the temperature and lensing signals are contributed by very different population of voids: the ISW signal is dominated by the large-scale gravitational potential, while the lensing convergence signal relates directly to density fluctuations on small scales.

### 3.3 Stacking with $3\sigma$ voids

Using 50 voids found from photometric redshift galaxies in the same volume as the CMASS sample, Granett et al. (2008; G08) found a temperature decrement of approximately  $-10\mu\text{K}$  at the  $3.7\sigma$  level. It is interesting to see if this result is also seen when using voids defined from spectroscopic data. We therefore follow the same selection criterion as G08, which was to select only voids that pass a  $3\sigma$  significance threshold; doing so reduces our void sample by a factor of 20. We apply the same selection criteria for our simulated voids and repeat the stacking analysis as in the previous subsection. Results are shown in Fig. 4.

For the stacked  $\Delta T$  measurement shown in the left-hand panel, the  $3\sigma$  voids display a trough between  $r_v = 100$  and  $150 h^{-1}\text{Mpc}$  that is similar to the one shown in Fig. 2, where all voids are used in the stacking. This is not surprising because there is a strong correlation between radius and significance for voids defined using ZOBOV: large voids tend to be more significant, so the

population of large voids is only slightly affected by the  $3\sigma$  selection. In fact, the selection slightly increases the amplitude of  $\Delta T$  at the trough, suggesting that the selection may have eliminated some voids that do not induce a large ISW signal. Once again, there is no significant signal at  $r_v > 150 h^{-1}\text{Mpc}$  – either in data or in simulation. As mentioned before, this is probably because the largest voids tend to be irregularly shaped, comprising a few density depressions. The volume centroid could align poorly with the density minimum for such a void. Ironically, photo- $z$  smearing could have alleviated this problem for the particular case of volume-centroided ZOBOV voids in G08, since smearing would have erased the substructure in the biggest voids, possibly making voids more regularly shaped, even if they are composed of a few subvoids.

Most small voids do not survive the high-significance threshold selection, as indicated by the bottom-left panel of Fig. 1, but the stacked properties of these few remaining objects are puzzling. We find that the filtered temperature crosses zero at  $r_v \approx 75 h^{-1}\text{Mpc}$ , while the simulated version approaches zero at  $r_v \approx 60 h^{-1}\text{Mpc}$ . There is then a noticeable positive  $\Delta T$  at  $r_v \approx 40 h^{-1}\text{Mpc}$  contributed by less than 30 voids, with an estimated  $2.5\sigma$  significance. This is not seen in our simulation, although we have even fewer voids in this regime due to the fact that the volume of our simulation is a factor of 2 smaller. We therefore lack the statistical power to be able to say whether this small-scale signal is simply a fluke, or whether it reflects some problem with the void sample. In fact, as shown by the grey circles in Fig. 6, there is a hint that some of these small voids might be affected by the survey boundary – e.g. the cluster of voids near Declination zero. In any case, because the predicted signal in this regime is close to zero, these small voids have very limited impact on the likelihood. As demonstrated in the bottom-left panel of Fig. 4, we reject zero  $\Delta T$  signal at  $3.7\sigma$  ( $3.4\sigma$  when neglecting void-to-void covariance) when all the selected voids are included. When we exclude voids smaller than  $r_v = 60 h^{-1}\text{Mpc}$ , motivated by the simulation results, the significance increases by only  $0.5\sigma$ . With or without the smallest voids, the formal rejection of the unscaled simulation predictions ( $\alpha = 1$ ) is almost as strong as the rejection of zero signal, and the preferred scaling is close to  $\alpha = 20$  – thus hugely inconsistent with  $\Lambda\text{CDM}$ , in agreement with the original finding of G08. This can be seen in more detail in Fig. 5, which shows the stacked temperature map that results when we restrict ourselves to only the largest  $3\sigma$  voids, with  $r_v > 100 h^{-1}\text{Mpc}$ . In the left-hand panel, a cold spot in the temperature map is apparent near the centre. The profile decreases towards the centre, with a steep transition from zero to negative at approximately  $0.7r_v$ . But the depth of this profile is completely inconsistent with the prediction, shown as the dotted line in the right-hand panel. We discuss this further in the next subsection.

Finally, we repeat the same analysis with the lensing  $\kappa$  map. We find that the result is consistent with a null signal overall. There is a single discrepant bin, centred on  $60 h^{-1}\text{Mpc}$ , which shows a  $>3\sigma$  deviation from zero; but such a signal is entirely absent from the surrounding bins. Since there was no reason to pick out this bin in advance, we can only see it as a statistical fluke. The average lensing profile for the larger  $3\sigma$  voids (with  $r_v > 100 h^{-1}\text{Mpc}$ ) is shown in Fig. 5: it actually matches the predictions very well, including the central dip of  $\kappa \approx -0.001$ , but the errors are too large to claim a detection. This lack of a lensing detection is not unexpected as we have seen from Fig. 2 that the lensing signal is contributed mainly by relatively small voids, and their number is significantly reduced by the  $3\sigma$  cut. But it is worth noting that the lensing map shows no hint of the large signal seen in temperature



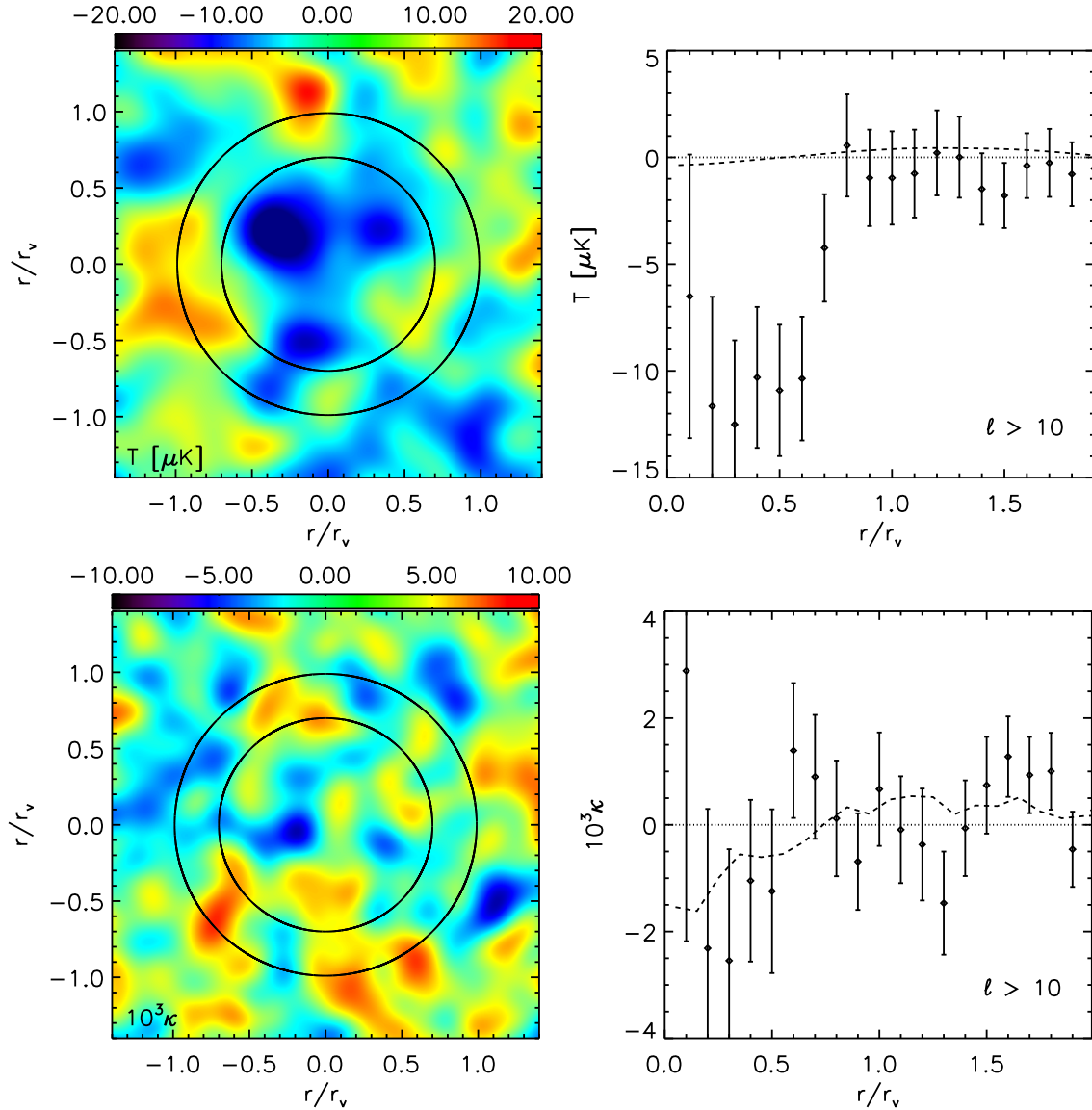


**Figure 5.** Left: Stacked Planck SEVEM map temperature maps (top) and Planck lensing  $\kappa$  maps (bottom) using  $3\sigma$  voids with  $r_v > 100 h^{-1}\text{Mpc}$  from the SDSS-DR12 CMASS galaxy catalogue. CMB maps are rescaled by the void radius  $r_v$  before stacking. The inner and outer circles have radii of  $r_v/\sqrt{2}$  and  $r_v$  respectively, representing the optimal filter radius we found from the HOD mock. ‘Up’ is the direction of Galactic north. Right: 1D temperature profile (top) and  $\kappa$  (bottom) profile for the left panels. The dashed curves are predictions from simulations of a  $\Lambda$ CDM model.

around  $r_v \approx 100 h^{-1}\text{Mpc}$ . This alone cautions against acceptance of the temperature effect as a true physical phenomenon: lensing depends on the potential sum  $\Phi + \Psi$ , whereas ISW depends on the time derivative of this quantity. It would seem unnatural for the time derivative to exceed the standard model by an order of magnitude without the value of the potentials themselves also suffering a substantial change. It is possible in principle to achieve such an effect in modified gravity models containing a rapidly oscillating scalar field, which is a feature for some models when the quasi-static approximation is dropped (e.g. Llinares & Mota 2014; Sawicki & Bellini 2015; Winther & Ferreira 2015), although then the ISW effect would not have a consistent amplitude at all redshifts.

### 3.4 Comparison with G08 results

We have seen that the trough of  $\Delta T$  from this  $3\sigma$  spectroscopic void sample is very close to that of G08, i.e.  $-8 \mu\text{K}$  from this study versus  $-10 \mu\text{K}$  in G08. The overall significance of these two measurements are also comparable, i.e.  $3.4\sigma$  from our conservative estimate versus  $3.7\sigma$  in G08. The significance of our measurement is contributed mostly by voids with  $60 < r_v < 150 h^{-1}\text{Mpc}$ , and the same is also true for G08. But G08 found that their mean stacked void signal was  $2\sigma$  above theoretical expectation, which was estimated to be  $-4.2 \mu\text{K}$ . In contrast, while our measurement is very similar to that of G08 in terms of both the amplitude and significance of deviation from null, our estimated ISW signal from the  $\Lambda$ CDM simulation is one order of magnitude lower, with the peak of its amplitude at the sub- $\mu\text{K}$  level. The value of  $-4.2 \mu\text{K}$  was found in G08 by centring a  $100 h^{-1}\text{Mpc}$  aperture around the maximum ISW signal in the Millennium simulation. This is the most

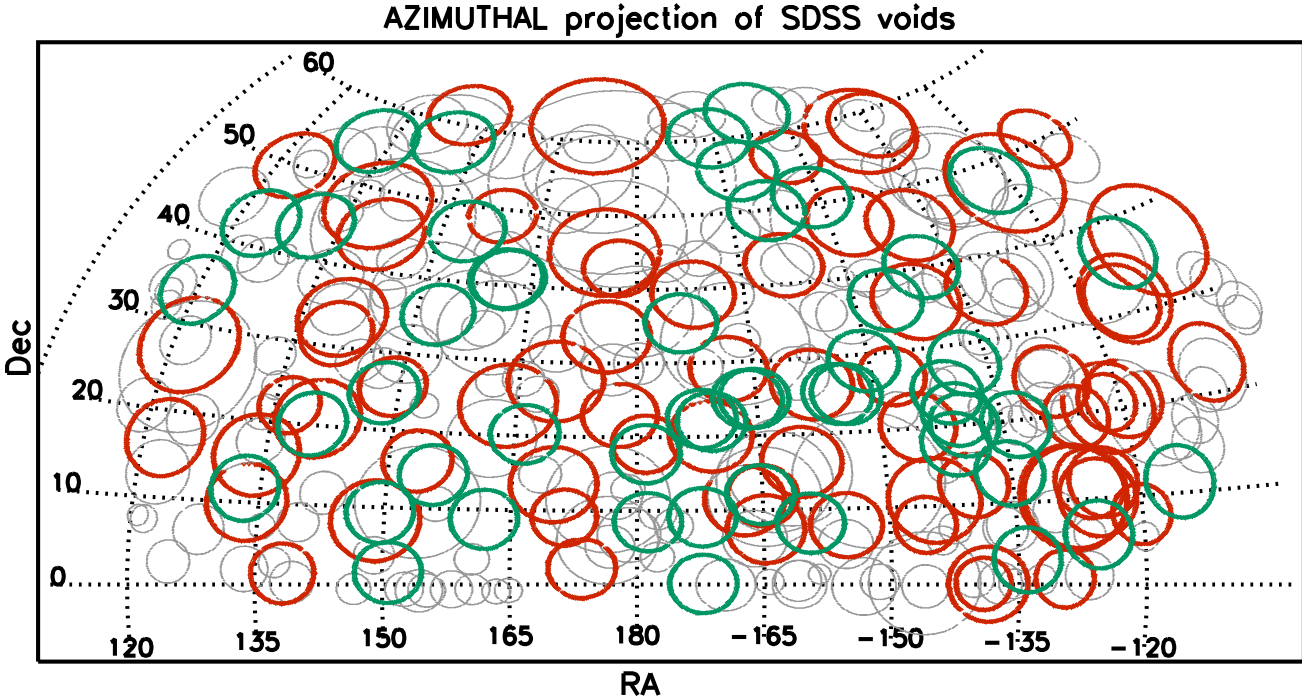


**Figure 6.** Comparing sky coordinates (RA & Dec) between the 50 DR6 voids from G08 versus those from DR12. Green circles with the radius of 4 degree (the size of the filter used in G08) represent the DR6 voids. Grey circles are all CMASS voids passing the  $3\sigma$  selection, a subset of which having  $r_v > 100 h^{-1} \text{Mpc}$  are shown in red. There are fewer than 10 overlaps between these two samples, which is 20% of the DR6 sample and less than 3% of the DR12 void sample. The green circles are DR12 voids with  $r_v > 100 h^{-1} \text{Mpc}$ , only 3 of which have a DR6 void at their vicinities.

optimistic case because the amplitude of the estimated ISW signal is not complicated by the process of void definition. But as we have demonstrated at the bottom-right panel of Fig. 1, simulated CMASS voids may not necessarily be very deep, and for the very large voids they may not correspond to real underdensities of dark matter. The amplitude of the simulated ISW effect associated with these voids can therefore be very different from the peak of the ISW signal in the simulation box. Similarly, any analytical calculation of the ISW signal using idealised void density profile may also be over-optimistic, unless the shape, and perhaps more importantly the depth of the assumed voids profile are closely matched to those found using the same void finding algorithm used in simulations and in observation.

Another difference with respect to G08 may be that our sets of  $3\sigma$  voids are not really that similar. Owing to photo- $z$  errors, there are very few voids with  $r_v < 60 h^{-1} \text{Mpc}$  in G08. Perhaps for the same reason, sub-voids derived using a photo- $z$  galaxy sample do not link up into main voids as much as in a spec- $z$  sample. The consequence is that no void with  $r_v > 140 h^{-1} \text{Mpc}$  can exist in G08, and their average void radius was about  $100 h^{-1} \text{Mpc}$ . In any case, when we compare the sky coordinates of these two void catalogues (Fig. 6), we find fewer than 10 close pairs or overlaps. This is less than 20% of the G08 sample and 3% of the CMASS sample. Therefore, it is not clear that we should expect as good an agreement in the observations as was actually achieved.

Given the lack of overlap between the our  $3\sigma$  voids and the list used by G08, it appears that the combination of these two samples might yield a more significant  $\Delta T$  measurement, in even stronger tension with  $\Lambda \text{CDM}$ . Because of the large-scale nature of the ISW effect, however, the precise degree of independence of the two re-

sults is difficult to quantify. But in any case, we have certainly produced no evidence to argue against the signal claimed by G08, which remains as puzzling as ever. The broader results in our paper suggest that the G08 result is heavily influenced by their decision to select  $3\sigma$  voids, rather than some other threshold. But there is no suggestion that G08 experimented with different thresholds so there is no scope for a ‘look elsewhere’ effect in assessing the significance of the signal. It seems unsatisfactory to dismiss a signal at this level as being simply a statistical fluke, but at present it seems the most plausible hypothesis, given the lack of a correspondingly strong lensing signal, plus the lack of a signal at the G08 level in our larger DR12 catalogue.

#### 4 SUMMARY AND CONCLUSIONS

By taking voids at  $0.4 < z < 0.7$  from the DR12 SDSS CMASS galaxy sample, and using Planck CMB data, we have measured the stacked CMB temperature ( $\Delta T$ ) and lensing convergence ( $\Delta \kappa$ ) at the void locations. An important aspect of our analysis is to use  $N$ -body simulations to calibrate the void catalogue, which enables us to select voids with physical motivation without introducing *a posteriori* bias. We have demonstrated that the simulated voids are good matches to the CMASS void data in terms of abundance, but the simulations also indicate that some of the catalogued voids are not true matter underdensities – particularly the largest systems, with  $r_v \gtrsim 150 h^{-1} \text{Mpc}$ . In this way, we have found the following results concerning the imprint of voids on the CMB:

(1) There is a relatively low ( $2.3\sigma$ ) significance for the void-CMB temperature cross-correlation, which is contributed mainly

by large voids with radii greater than  $100 h^{-1}\text{Mpc}$ . The void-CMB lensing association is much stronger, at the  $3.2\sigma$  level, contributed mostly by smaller voids. Thus we do not detect simultaneous temperature and lensing imprints from the same set of voids. This is not unexpected: if  $\Delta T$  is induced by the ISW effect, it would arise from the decay of the gravitational potential, which is a smoothed version of the density field, while the lensing convergence map comes directly from the projected matter density.

(2) When interpreted as the ISW signal, our measured  $\Delta T$  is a few times larger than expected from a  $\Lambda\text{CDM}$  model (although not strongly inconsistent statistically with the standard-model prediction); but the amplitude of the lensing  $\Delta\kappa$  is a very good match to  $\Lambda\text{CDM}$ . Moreover, the projected void profile from observation is consistent with that from our simulations. For the larger voids that show the tentative ISW signal, there is no indication of an enhanced amplitude for the lensing signal; this is of the order of  $\Delta\kappa \sim 10^{-3}$  and well within the statistical errors of the Planck lensing map.

(3) Our measurement of the stacked void profile is the first to use CMB lensing data; this is more efficient for voids at high redshift, where measurements of weak galaxy lensing are challenging. The good agreement of void abundances between observation and simulations plus the agreement between the observed and simulated void profiles suggest that the detected CMB lensing signal is robust. Accurate measurement of void profiles may provide valuable information for cosmology and gravity. Dark matter void profiles evolve differently in different cosmologies (Demchenko et al. 2016); in certain type of modified gravity, e.g. those with the chameleon screening mechanism, voids are expected to be emptier than their GR counterparts. The dark matter profile of voids can therefore provide powerful test for modified gravity (Clampitt et al. 2013; Lam et al. 2015; Cai et al. 2015; Barreira et al. 2015). Our measurement suggests that it is possible to do this with CMB lensing.

(4) When repeating the same analyses, removing voids of lower statistical significance gives a null detection in lensing, but the measured  $\Delta T$  becomes more strongly non-zero. The amplitude of  $\Delta T$  and its significance are both similar to those reported in Granett et al. (2008) for voids of this strength. The crucial (and only) factor leading to this result is the selection of voids that are  $3\sigma$  deviations in terms of Poisson fluctuations, as in Granett et al. (2008). The level of the temperature signal remains puzzling: for large voids ( $r_v \approx 125 h^{-1}\text{Mpc}$ ), we find it to be about 20 times the  $\Lambda\text{CDM}$  prediction (albeit with a large uncertainty), which is a larger discrepancy than claimed by Granett et al. (2008). Conversely, there is a *positive* temperature deviation for voids with  $r_v \lesssim 60 h^{-1}\text{Mpc}$ , which is qualitatively incompatible with our simulations. Such gross discrepancies are not seen in our larger sample of DR12 voids, nor do we see a boosted signal in the lensing by voids (with or without  $3\sigma$  thresholding). It therefore seems unlikely that this anomalous temperature result can really be taken as evidence that standard gravity is in error. In particular, our measurements of void lensing argue that  $\Lambda\text{CDM}$  is a good match to observation, even though the temperature signal in this rare void subset remains to be better understood.

**ACKNOWLEDGEMENTS**

We thank Baojiu Li for providing the  $N$ -body simulation used for this study. YC was supported during this work by funding from an STFC Consolidated Grant. YC and JAP were supported by ERC grant number 670193. MN was supported at IAP under the ILP LABEX (ANR-10-LABX-63) supported by French state funds managed by the ANR within the Investissements d'avenir programme under reference ANR-11-IDEX-0004-02, and also by ERC Project No. 267117 (DARK) hosted by Université Pierre et Marie Curie (UPMC) Paris 6, PI J. Silk. MN was supported at Durham by the UK Science and Technology Facilities Council [ST/L00075X/1]. QM and AAB were supported in part by the National Science Foundation (NSF) through NSF Career Award AST-1151650.

**REFERENCES**

- Amendola L., Frieman J. A., Waga I., 1999, *MNRAS*, 309, 465  
 Barreira A., Cautun M., Li B., Baugh C. M., Pascoli S., 2015, *JCAP*, 8, 028  
 Berlind A. A., Weinberg D. H., 2002, *ApJ*, 575, 587  
 Cai Y.-C., Cole S., Jenkins A., Frenk C., 2009, *MNRAS*, 396, 772  
 Cai Y.-C., Cole S., Jenkins A., Frenk C. S., 2010, *MNRAS*, 407, 201  
 Cai Y.-C., Neyrinck M. C., Szapudi I., Cole S., Frenk C. S., 2014, *ApJ*, 786, 110  
 Cai Y.-C., Padilla N., Li B., 2015, *MNRAS*, 451, 1036  
 Clampitt J., Cai Y.-C., Li B., 2013, *MNRAS*, 431, 749  
 Clampitt J., Jain B., 2015, *MNRAS*, 454, 3357  
 Cuesta A. J., Vargas-Magaña M., Beutler F., Bolton A. S., Brownstein J. R., Eisenstein D. J., Gil-Marín H., Ho S., McBride C. K., et al. 2016, *MNRAS*, 457, 1770  
 Dawson K. S., Schlegel D. J., Ahn C. P., Anderson S. F., Aubourg É., Bailey S., Barkhouser R. H., Bautista J. E., et al. 2013, *AJ*, 145, 10  
 Demchenko V., Cai Y.-C., Heymans C., Peacock J. A., 2016, *ArXiv: 1605.05286*  
 Eisenstein D. J., Weinberg D. H., Agol E., Aihara H., Allende Prieto C., Anderson S. F., Arns J. A., Aubourg É., Bailey S., Balbinot E., et al. 2011, *AJ*, 142, 72  
 Granett B. R., Kovács A., Hawken A. J., 2015, *arXiv:1507.03914*  
 Granett B. R., Neyrinck M. C., Szapudi I., 2008, *ApJ*, 683, L99  
 Granett B. R., Neyrinck M. C., Szapudi I., 2009, *ApJ*, 701, 414  
 Gruen D., Friedrich O., Amara A., Bacon D., Bonnett C., Hartley W., Jain B., Jarvis M., et al. 2016, *MNRAS*, 455, 3367  
 Higuchi Y., Oguri M., Hamana T., 2013, *MNRAS*, 432, 1021  
 Hotchkiss S., Nadathur S., Gottlöber S., Iliev I. T., Knebe A., Watson W. A., Yepes G., 2015, *MNRAS*, 446, 1321  
 Ilić S., Langer M., Douspis M., 2013, *A&A*, 556, A51  
 Krause E., Chang T.-C., Doré O., Umetsu K., 2013, *ApJ*, 762, L20  
 Lam T. Y., Clampitt J., Cai Y.-C., Li B., 2015, *MNRAS*, 450, 3319  
 Li B., Hellwing W. A., Koyama K., Zhao G.-B., Jennings E., Baugh C. M., 2013, *MNRAS*, 428, 743  
 Llinares C., Mota D. F., 2014, *Phys. Rev. D*, 89, 084023  
 Manera M., Scoccimarro R., Percival W. J., Samushia L., McBride C. K., Ross A. J., Sheth R. K., White M., et al. 2013, *MNRAS*, 428, 1036  
 Mao Q., et al. 2015, *arXiv:1602.02771*  
 Melchior P., Sutter P. M., Sheldon E. S., Krause E., Wandelt B. D., 2014, *MNRAS*, 440, 2922  
 Nadathur S., Hotchkiss S., 2015, *arXiv:1504.06510*  
 Neyrinck M. C., 2008, *MNRAS*, 386, 2101  
 Neyrinck M. C., Gnedin N. Y., Hamilton A. J. S., 2005, *MNRAS*, 356, 1222  
 Peacock J. A., Smith R. E., 2000, *MNRAS*, 318, 1144  
 Planck Collaboration Ade P. A. R., Aghanim N., Armitage-Caplan C., Arnaud M., Ashdown M., Atrio-Barandela F., Aumont J., Baccigalupi C., Banday A. J., et al. 2014, *A&A*, 571, A19  
 Planck Collaboration Adam R., Ade P. A. R., Aghanim N., Alves M. I. R., Arnaud M., Ashdown M., Aumont J., Baccigalupi C., Banday A. J., et al. 2015a, *arXiv:1502.01588*  
 Planck Collaboration Ade P. A. R., Aghanim N., Arnaud M., Ashdown M., Aumont J., Baccigalupi C., Banday A. J., Barreiro R. B., Bartlett J. G., et al. 2015b, *arXiv:1502.01591*  
 Planck Collaboration Ade P. A. R., Aghanim N., Arnaud M., Ashdown M., Aumont J., Baccigalupi C., Banday A. J., Barreiro R. B., Bartolo N., et al. 2015c, *arXiv:1502.01595*  
 Planck Collaboration Aghanim N., Arnaud M., Ashdown M., Aumont J., Baccigalupi C., Banday A. J., Barreiro R. B., Bartlett J. G., Bartolo N., et al. 2015d, *arXiv:1502.01596*  
 Planck Collaboration Adam R., Ade P. A. R., Aghanim N., Arnaud M., Ashdown M., Aumont J., Baccigalupi C., Banday A. J., Barreiro R. B., et al. 2015e, *arXiv:1502.05956*  
 Rees M. J., Sciama D. W., 1968, *Nature*, 217, 511  
 Sachs R. K., Wolfe A. M., 1967, *ApJ*, 147, 73  
 Sánchez C., Clampitt J., Kovacs A., Jain B., García-Bellido J., Nadathur S., Gruen D., Hamaus N., et al. 2016, *arXiv:1605.03982*  
 Sawicki I., Bellini E., 2015, *Phys. Rev. D*, 92, 084061  
 Scoccimarro R., Sheth R. K., Hui L., Jain B., 2001, *ApJ*, 546, 20  
 Seljak U., 1996, *ApJ*, 460, 549  
 Seljak U., 2000, *MNRAS*, 318, 203  
 Sheth R. K., van de Weygaert R., 2004, *MNRAS*, 350, 517  
 Smith R. E., Hernández-Monteagudo C., Seljak U., 2009, *Phys. Rev. D*, 80, 063528  
 White M., Blanton M., Bolton A., Schlegel D., Tinker J., Berlind A., da Costa L., Kazin E., et al. 2011, *ApJ*, 728, 126  
 Winther H. A., Ferreira P. G., 2015, *Phys. Rev. D*, 92, 064005  
 Zheng Z., Berlind A. A., Weinberg D. H., Benson A. J., Baugh C. M., Cole S., Davé R., Frenk C. S., Katz N., Lacey C. G., 2005, *ApJ*, 633, 791